Comparison of VLP-16 and MRS-1000 LiDAR systems with absolute interferometer

Comparison of VLP-16 and MRS-1000 LiDAR systems with absolute interferometer

1st Davide Cassanelli
Dep. of Engineering "E. Ferrari"
University of Modena and R. Emilia
Modena, Italy
davide.cassanelli@unimore.it

2st Stefano Cattini
Dep. of Engineering "E. Ferrari"
University of Modena and R. Emilia
Modena, Italy
stefano.cattini@unimore.it

3st Giorgio Di Loro
Dep. of Engineering "E. Ferrari"
University of Modena and R. Emilia
Modena, Italy
giorgio.diloro@unimore.it

4st Luca Di Cecilia
CNH Industrial
Modena, Italy
luca.dicecilia@cnhind.com

5st Luca Ferrari
CNH Industrial
Modena, Italy
luca.ferrari@cnhind.com

6st Luigi Rovati
Dep. of Engineering "E. Ferrari"
University of Modena and R. Emilia
Modena, Italy
luigi.rovati@unimore.it

***Abstract*—Nowadays, LiDARs hold a relevant place in providing the environmental sensing required by most ADAS. Promoted by such increasing demand, many new manufacturers are emerging and, new LiDARs are continuously made available on the market. If, on the one hand, the availability of LiDARs with increasing performance and reducing cost has brought significant benefits also promoting the spread of such measuring systems in other areas such as industrial controls and agriculture, on the other, it has made it more difficult to extricate in the immense set of LiDARs present on the market today. In response to this growing need for standards and methods capable of comparing the various LiDARs, many international standards and scientific publications are being produced on the subject. In this paper, we continue our work on LiDARs characterization, focusing our attention on comparing the performances of two of the most popular systems — namely, the MRS 1000 by Sick and the VLP 16 by Velodyne. Starting from the analysis of the warm-up time and stability, such a comparison focused on analyzing the axial error of both systems. Such errors have been estimated by exploiting a custom rail system and an absolute interferometer. The obtained results revealed warm-up times of a few tens of minutes and maximum absolute axial errors of a few centimeters in the range $[1.5, 21]$ m.**

***Index Terms*—LiDAR, LADAR, ToF, Terrestrial laser scanner, Measurement, Autonomous driving, ADAS.**

I. Introduction

Advanced driver assistance systems (ADASs) are nowadays more and more present on cars. If until a few years ago they were mainly reserved for high-end cars, nowadays they are increasingly present in utilitarian cars too. Indeed, ADASs and autonomous driving are recognized among the major drivers of change in the next future of the automotive sector. In this scenario, LiDARs hold a relevant place in providing the environmental sensing required by most ADASs and essential for autonomous driving [1].

Promoted by the increasing demand, LiDARs manufacturers are thus continuously proposing new measuring systems better performing both in terms of metrological properties and cost. Such has also fostered the diffusion of LiDARs in new areas such as, for example, industrial controls and agriculture. The availability of more and more LiDARs with increasing performance and reducing cost is thus bringing significant benefits in many respects. On the other hand, however, it is making increasingly difficult to disentangle the wide range of LiDARs on the market today. In response to this growing need for assessing and benchmarking the various LiDARs, many international standards and scientific publications are being produced on the subject [2]–[11].

In this paper, we pay our attention to the comparison of the performances of two of the most popular LiDAR systems, namely the MRS 1000 by Sick and the VLP 16 by Velodyne. Starting from the measurement procedure proposed in our recent paper [11], we investigated and compared warm-up time, stability, and error in the axial-measure. In addition, in this article we also analyze the stability of the signal strength received by the LiDAR.

In the following, Section II briefly recalls the proposed measurement procedure. Then, in Section III, we present the results obtained from both the measuring systems and finally, in Section IV we conclude with some considerations on the results obtained and on future applications.

II. Materials and Methods

As described in more detail in our recent paper [11], the analysis of the LiDARs performances is based on the custom rail system shown in Fig. 1. Realized with aluminum profiles, such a rail allows translating a plane target along the axis of the IUT (Instrument Under Test). In particular, the reported test have been performed exploiting a 24" by 24" hardboard target (model TB4 by Thorlabs) whose spectral reflectance is shown in Fig. 2. Such a target can be translated along the rail to obtain the axial distance, d, between the IUT and the target to vary in the range $d \in [1.5, 21]$ m. As shown in Fig. 3, the axial distance estimated by the IUT was thus compared with the distance, d_{INT}, estimated by the absolute interferometer INT (model HP5527A by HP).

To make the alignment between the IUT and the rail more

easy and accurate, the IUT was fixed on a multi-axis stage. Then, IUT, INT, and rail were aligned following the procedure described in [11]. The result of the alignment procedure was to obtain the z-axis of the IUT and the measuring axis of the INT nominally parallel to the axis defined by the rail with a maximum misalignment between the z-axis of the IUT and the measuring axis of the INT reasonably within $[-1.6, 1.6]^\circ$ [11]. Moreover, after the alignment procedure, the z-axis of the IUT is orthogonal to the plane identified by the target and intercepts it approximately at the center of the target.

To minimize possible effects due to ambient temperature and illumination, the rail was positioned in an environment with controlled temperature and lighting.

In the following, subsections II-A e II-B introduce the procedures exploited to investigate warm-up time, stability, and axial-error. The instruments settings exploited in all the analysis are resumed in Table I.

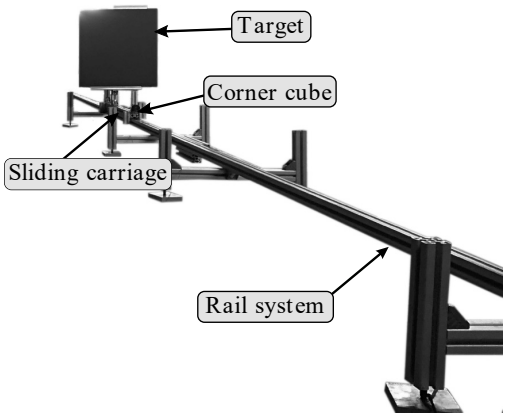

Fig. 1. Picture of the custom-designed aluminum rail system used for the LiDARs characterization. In the image are recognizable a portion of the rail, the sliding carriage, onto which the target is fixed, and the corner-cube, that together with the interferometer was used to estimate the target distance.

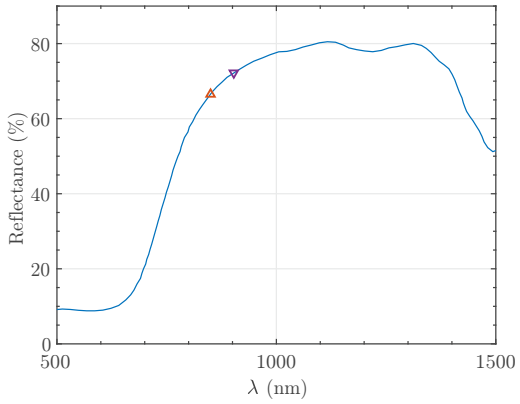

Fig. 2. Spectral reflectance of the target (model TB4 by Thorlabs) declared by the manufacturer. Symbols represent the reflectances at the nominal emission wavelength of MRS 1000 (850 nm, △), and, VLP 16 (903 nm, ▽), respectively. As shown in the figure, the target reflectance for MRS 1000 is about 67%, whereas the reflectance for VLP 16 is about 72%.

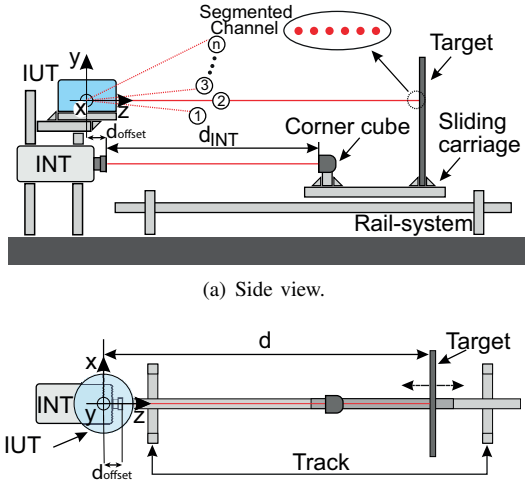

(a) Side view.

(b) Top view.

Fig. 3. Principle scheme of the setup shown in figure Fig. 1. Moving the carriage along the rail, it is possible to modify the IUT to target distance, d. The corner-cube fixed to the carriage is used by the interferometer INT to estimate such a distance. The origin of the Cartesian system, x, y, z, coincides with the IUT origin. Acting on the multi-axis stage, the IUT is aligned to the rail so that the z-axis is parallel to it. d_{offset} is the distance between the origins of the interferometer and the IUT along the z-axis.

TABLE I
INSTRUMENTS SETTINGS.

LiDAR	Value
MRS 1000 by Sick	Scanning frequency f_{scan} 50 Hz (fixed) Filter None HDDM+ OFF
VLP 16 by Velodyne	Scanning frequency f_{scan} 10 Hz Laser Return Modes: Single, Strongest

A. *Warm-up and Stability*

Instrument warm-up analysis is always one of the first characterizations that must be performed. Given that as the distance d increases, the number of points on the target decreases, warm-up and stability were analyzed by positioning the target at a distance $d \approx 6.5$ m. Then, the following procedure was used for each of the two IUT. The IUT was set to log a point-cloud every minute. Subsequently, after keeping it off for at least 12 hours, the IUT was turned on, starting the acquisition of 720 point-cloud.

At the end of the measurement session the acquired point-clouds were segmented to analyze the points on the target relating to a single IUT channel. For each of the IUT, the sets of points after segmentation are referred as $P(t)$, where t is the time since IUT was switched on.

Since the two IUT have different horizontal angular resolution, the same analyzed target area gave rise to a different number of points. Indeed, the cardinality N_t of $P(t)$ was N_t = 23 for the VLP 16 and, N_t = 16 for the MRS 1000. Note that each point of the point-cloud is a four-dimensional vector containing the Cartesian coordinates of the point and the intensity, I, of the detected signal. Hence, for each $P(t)$ we analyzed the mean z, the mean I and, their experimental standard deviations of

the mean:

$$\begin{aligned}
\bar{z}(t) &= \frac{1}{N_t} \cdot \sum_{i=1}^{N_t} z_i(t) \ , \\
\bar{I}(t) &= \frac{1}{N_t} \cdot \sum_{i=1}^{N_t} I_i(t) \ , \\
s_{\bar{z}}(t) &= \sqrt{\frac{1}{N_t(N_t-1)} \sum_{i=1}^{N_t} \Big[z_i(t) - \bar{z}(t) \Big]^2} \\
s_{\bar{I}}(t) &= \sqrt{\frac{1}{N_t(N_t-1)} \sum_{i=1}^{N_t} \Big[I_i(t) - \bar{I}(t) \Big]^2},
\end{aligned} \tag{1}$$

where, as previously introduced, N_t is the cardinality of $P(t)$. Since the amplitudes of the standard deviations $s_{\bar{z}}(t)$ and $s_{\bar{I}}(t)$ were not negligible compared to the amplitudes of the fluctuations of the respective mean values $\bar{z}(t)$ and $\bar{I}(t)$, the warm-up times have been defined exploiting decision rules similar to the ''guarded acceptance" and "guarded rejection" described in JCGM 106:2012 [12] for conformity assessment. Hence, as described in more detail in [10], we defined two guard bands centered around the upper and lower tolerance limits (T_U and T_L) and having a half-width amplitude equal to the experimental standard deviation of the mean. Both for the intensity I and the distance z, the upper limit of the warm-up time, t_{warm-U}, was thus estimated as the time it was required to the mean value, $\bar{z}(t)$ or $\bar{I}(t)$, to stay within the upper tolerance interval (UTI) obtained symmetrically reducing the $[T_L, T_U]$ range of twice the experimental standard deviation of the mean — UTI = $[T_L + s(t), T_U - s(t)]$, where $s(t)$ represents $s_{\bar{z}}(t)$ or $s_{\bar{I}}(t)$. Similarly, the lower limit of the warm-up time, t_{warm-L}, was obtained analyzing the time required to the mean value to stay within the lower tolerance interval (LTI) obtained symmetrically expanding the $[T_L, T_U]$ range of twice the experimental standard deviation of the mean LTI = $[T_L - s(t), T_U + s(t)]$. Consequently, a range of values of warm-up times was obtained both for the intensity I and, the distance z. Assuming that warm-up times relative to z and I end respectively in the first n_{w-z} and n_{w-I} samples obtained considering the respective t_{warm-U}, the stability has been investigated in terms of experimental standard deviations

$$\begin{aligned}
s_{\bar{z}-steady} &= \sqrt{\frac{1}{n_{TOT} - n_{w-z} - 1} \sum_{i=n_{w-z}}^{n_{TOT}} \Big[\bar{z}(i) - \bar{z}_{steady} \Big]^2} \\
s_{\bar{I}-steady} &= \sqrt{\frac{1}{n_{TOT} - n_{w-I} - 1} \sum_{i=n_{w-I}}^{n_{TOT}} \Big[\bar{I}(i) - \bar{I}_{steady} \Big]^2} \ ,
\end{aligned} \tag{2}$$

where $n_{TOT} = 720$ is the total number of recorded point-clouds and

$$\begin{aligned}
\bar{z}_{steady} &= \frac{1}{n_{TOT} - n_{w-z}} \cdot \sum_{i=n_{w-z}}^{n_{TOT}} \bar{z}(i) \ , \\
\bar{I}_{steady} &= \frac{1}{n_{TOT} - n_{w-I}} \cdot \sum_{i=n_{w-I}}^{n_{TOT}} \bar{I}(i) \ .
\end{aligned} \tag{3}$$

B. Comparison with interferometer

The analysis of the axial-error has been performed by using the setup shown in Figs. 1 and 3, thus translating the planar target along the rail-system to modify the IUT-target distance d. As previously described, the IUT, INT, and rail were aligned to obtain the z-axis of the IUT and the measuring axis of the INT nominally parallel to the axis defined by the rail and orthogonal to the plane identified by the target. Then, after having waited a time from switching on the instrument not less than the relative t_{warm-U}, we started the measurements. For each target distance, we thus acquired both a point-cloud from the IUT and a measure, $d_{INT}(d)$, from the interferometer INT.

Similar to what was done in the warm-up analysis, at the end of the measurement session the acquired point-clouds were segmented to analyze the points on the target relating to a single IUT channel. The sets of points after segmentation are referred as $P(d)$, where d is the IUT-target distance. Note that, as previously introduced, as the distance d increases, the number of points on the target decreases. Therefore, we considered only those rays that continued to fall on the target even when it was at the maximum distance $d \approx 21$ m. Hence, for each distance d, the $P(d)$ set consisted of the same number of points and the cardinality N_t of $P(d)$ was $N_t = 6$ for the VLP 16 and, $N_t = 4$ for the MRS 1000.

For each $P(d)$, we thus compute the mean distance and its experimental standard deviation of the mean:

$$\begin{aligned}
\bar{z}(d) &= \frac{1}{N_d} \cdot \sum_{i=1}^{N_d} z_i(d) \ , \\
s_{\bar{z}}(d) &= \sqrt{\frac{1}{N_d(N_d-1)} \sum_{i=1}^{N_d} \Big[z_i(d) - \bar{z}(d) \Big]^2} \ .
\end{aligned} \tag{4}$$

Note that, as shown in Fig. 3, although the plane identified by the corner-cube is parallel to the plane identified by the target, there is an offset between the two. Moreover, the position of the origin of the axes of the IUT and INT is not known and not even easily estimated. Hence, there is a fixed and unknown offset between the IUT to target distance, d, and the INT to corner-cube distance d_{INT}. Such an offset, d_{offset}, was estimated as the intercept of the linear interpolation between the $\bar{z}(d)$ and $d_{INT}(d)$. Then, the axial-error has been estimated as:

$$\text{Error}(d) = d_{INT}(d) + d_{offset} - \bar{z}(d) \ . \tag{5}$$

Estimating d_{offset} from the linear interpolation between $\bar{z}(d)$ and $d_{INT}(d)$, we compensated for any constant offset error affecting the IUT. Hence, (5) provides an estimate of the "best case" errors.

III. Results

A. Warm-up and Stability

Fig. 4 shows the results obtained from the analysis of the warm-up times relative to the distance estimate. Such an analysis has been performed setting the upper and lower

tolerance limits (T_U and T_L) at ±0.15% of the $\bar{z}_{steady}$ value. Similarly, Fig. 5 shows the results obtained from the analysis of the warm-up times relative to the intensity. Given the greater variability of the received intensity, $\bar{I}(t)$, compared to the distance $\bar{z}(t)$, the warm-up analysis for the intensity has been performed setting the upper and lower tolerance limits (T_U and T_L) at ±10% of the $\bar{I}_{steady}$ value.

As described in subsection II-A, the stability was analyzed by evaluating the point-clouds acquired after t_{warm-U}. The warm-up and stability tests results are resumed in Table II.

During the tests, the ambient temperature ranged from 18 °C to 20 °C, with a mean value of about 19 °C. Approximating the thermal expansion coefficient of aluminum to be $2.4{\cdot}10^{-5}$ K^{-1}, such resulted in a fractional change in the rail length that can be assumed irrelevant for the warm-up and stability analysis.

TABLE II
ESTIMATED WARM-UP TIMES AND STABILITY. $\gamma_z = s_{\bar{z}-steady}/\bar{z}_{steady}$ AND $\gamma_I = s_{\bar{I}-steady}/\bar{I}_{steady}$.

Parameter	$[t_{warm-L}, t_{warm-U}]$	Stability
MRS 1000 $\bar{z}$	$[3, 20]$ min	$\gamma_z = 3.6 \cdot 10^{-04}$
MRS 1000 $\bar{I}$	$[1, 9]$ min	$\gamma_I = 8.2 \cdot 10^{-03}$
VLP 16 $\bar{z}$	$[1, 20]$ min	$\gamma_z = 2.6 \cdot 10^{-04}$
VLP 16 $\bar{I}$	$[10, 11]$ min	$\gamma_I = 13.6 \cdot 10^{-03}$

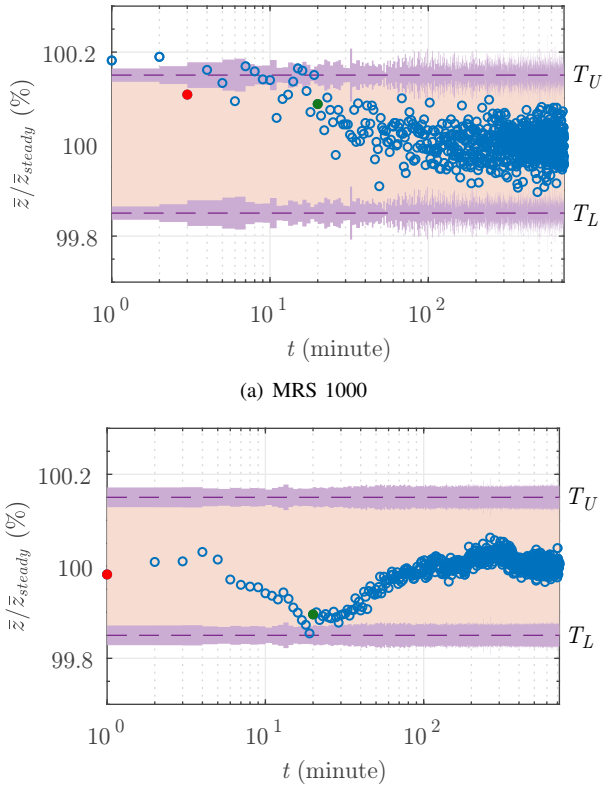

(a) MRS 1000

(b) VLP 16

Fig. 4. Analysis of the warm-up related to the distance estimate. The tolerance interval $[T_L, T_U]$, set at ±0.15% of $\bar{z}_{steady}$, is represented by the dashed lines (– – –), whereas the guard bands are represented by the purple areas. In both figures, the lower limit of the warm-up time, t_{warm-L}, is represented by a red bullet (•), whereas the upper limit of the warm-up time, t_{warm-U}, is represented by a green bullet (•).

B. Comparison with interferometer

Fig. 6 compares the distances $\bar{z}$ estimated by the two IUT and the distance estimated by the interferometer. Fig. 7 shows the errors estimated as defined in subsection II-B.

The results of the analysis of the axial-error are summarized in Table III.

During the test, the ambient temperature ranged from 18 °C to 21 °C, with a mean value of about 19 °C.

TABLE III
MEAN AND MAXIMUM ABSOLUTE ERRORS IN THE ESTIMATE OF THE AXIAL DISTANCE FOR THE MRS 1000 AND THE VLP 16.

LiDAR	Mean Error	Maximum Absolute Error
MRS 1000	3.9 mm	24.2 mm
VLP 16	-4.9 mm	-12.8 mm

IV. CONCLUSIONS

The availability of increasingly performing and lower costing measuring systems is promoting an ever-increasing pervasion of measurements in all areas. Automotive is no exception. Indeed, automotive has become one of the leading drivers of sensors development. The increasing diffusion of sensors in the automotive sector concerns both sensors installed onboard vehicles e.g. [1], [13], [14] and sensors that are installed along specific road sections e.g. [15]–[17]. In this scenario, LiDARs are becoming one of the pillars for environmental sensing needed in ADAS. LiDARs manufacturers are making available measuring systems increasingly performing both in terms of metrological characteristics and cost. Such has brought countless benefits, but it is also making more difficult for designers, who have to integrate such sensors into their systems, to compare and choose the most suitable LiDAR for their application. In response to a such growing need of assessing and benchmarking the various LiDARs, many international standards and scientific publications are being produced. In this paper, we continue our work on LiDARs characterization, focusing our attention on comparing the performances of two of the most popular systems — namely, the MRS 1000 by Sick and the VLP 16 by Velodyne.

The characterization of the two measuring systems, concerning warm-up time, stability and axial error referred to the interferometer, is being completed. The obtained results revealed warm-up times of a few tens of minute, related to the distance estimate, and about ten minute, related to the received intensity, for both the sensors. Moreover, the stability analysis reveals stability values similar between the two measuring systems. As shown in Fig.s4(a)4(b), the stability parameter γ_z, related to the distance estimate, is an order of magnitude lower with respect to the γ_I, for both the sensors. As shown in Fig. 7, concerning the measurement of the axial error respect of the interferometer, in the range of [1.5, 21] m, the MRS 1000 suffer from a higher maximum absolute axial error, respect the VLP 16, while the mean error is similar, and in the order

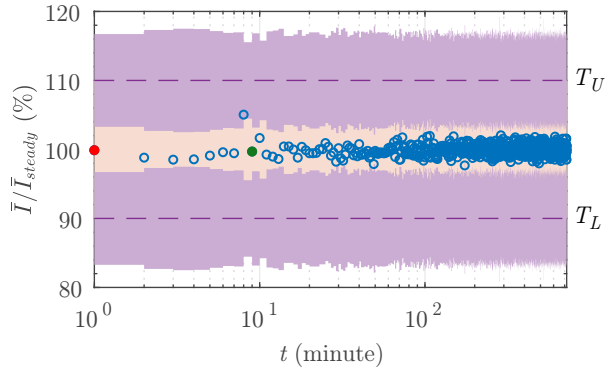

(a) MRS 1000

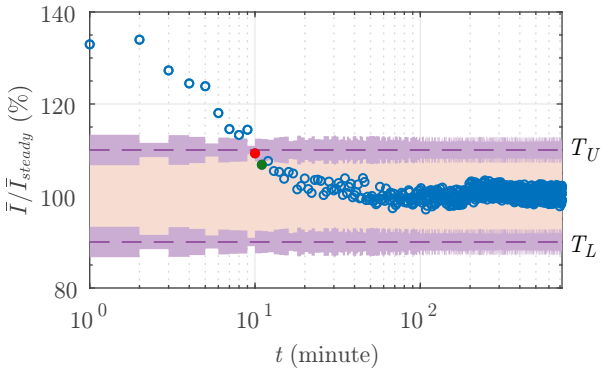

(b) VLP 16

Fig. 5. Analysis of the warm-up related to the received intensity. The tolerance interval $[T_L, T_U]$, set at ±10% of $\bar{I}_{steady}$, is represented by the dashed lines (– – –), whereas the guard bands are represented by the purple areas. In both figures, the lower limit of the warm-up time, t_{warm-L}, is represented by a red bullet (•), whereas the upper limit of the warm-up time, t_{warm-U}, is represented by a green bullet (•).

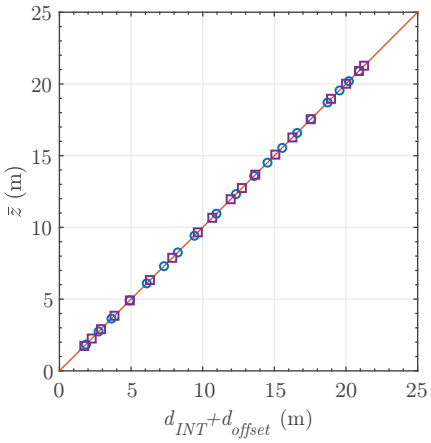

Fig. 6. Comparison of target distances measured by both the IUT and the interferometer. The circles (○) refer to the measurements of the MRS 1000, while the squares (□) refer to the measurements of the VLP 16. The bisector of the first quadrant (—) was added to guide the eyes.

of few millimeters for both systems.

The proposed article not only provides a comparison between two of the most popular LiDARs but also describes a simple and adaptable measurement procedure for LiDARs analysis.

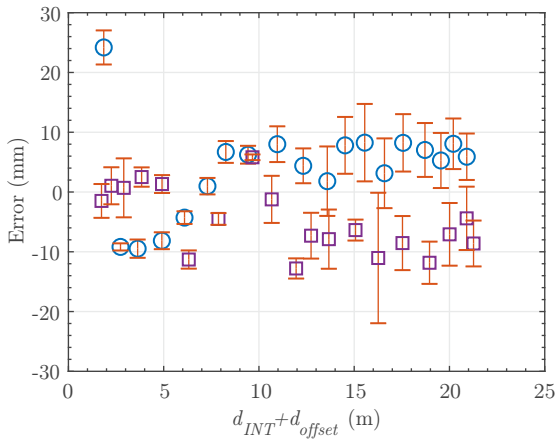

Fig. 7. Errors estimated according to (5). The circles (○) refer to the measurements of the MRS 1000, while the squares (□) refer to the measurements of the VLP 16. The vertical bars represent the respective experimental standard deviations of the mean $s_{\bar{z}}$.

Thus, it can support designers in the analysis and comparison of the many LiDAR systems that are continuously made available on the market.

References

[1] R. Thakur, "Scanning LIDAR in advanced driver assistance systems and beyond: Building a road map for next-generation LIDAR technology," *IEEE Consumer Electronics Magazine*, vol. 5, no. 3, pp. 48–54, July 2016.

[2] ASTM E3125-17, "Standard Test Method for Evaluating the Point-to-Point Distance Measurement Performance of Spherical Coordinate 3D Imaging Systems in the Medium Range," ASTM International, West Conshohocken, PA, USA, Tech. Rep., Tech. Rep., 2017. [Online]. Available: http://www.astm.org/cgi-bin/resolver.cgi?E3125-17

[3] ASTM E2938-15, "Standard test method for evaluating the relative range measurement performance of 3d imaging systems in the medium range," ASTM International, West Conshohocken, PA, USA, Tech. Rep., Tech. Rep., 2015. [Online]. Available: http://www.astm.org/cgibin/resolver.cgi?E293

[4] M. A. Cooper, J. F. Raquet, and R. Patton, "Range information characterization of the hokuyo ust-20lx lidar sensor," *Photonics*, vol. 5, no. 2, 2018. [Online]. Available: https://www.mdpi.com/2304-6732/5/2/12

[5] Z. Wang, Y. Liu, Q. Liao, H. Ye, M. Liu, and L. Wang, "Characterization of a rs-lidar for 3d perception," in *2018 IEEE 8th Annual International Conference on CYBER Technology in Automation, Control, and Intelligent Systems (CYBER)*, 2018, pp. 564–569.

[6] P. Rachakonda, B. Muralikrishnan, M. Shilling, D. Sawyer, and G. Cheok, "An Overview of Activities at NIST Towards the Proposed ASTM E57 3D Imaging System Point-to-point Distance Standard," *Journal of the CMSC*, vol. 12, no. 2, pp. 1–14, 2017. [Online]. Available: https://www.ncbi.nlm.nih.gov/pmc/articles/PMC6508635/

[7] P. Rachakonda, B. Muralikrishnan, L. Cournoyer, G. Cheok, V. Lee, M. Shilling, and D. Sawyer, "METHODS AND CONSIDERATIONS TO DETERMINE SPHERE CENTER FROM TERRESTRIAL LASER SCANNER POINT CLOUD DATA," *Measurement science & technology*, vol. 28, no. 10, Oct. 2017. [Online]. Available: https://www.ncbi.nlm.nih.gov/pmc/articles/PMC5992622/

[8] M. Tsakiri, V. Pagounis, and O. Arabatzi, "Evaluation of a pulsed terrestrial laser scanner based on iso standards," *Surface Topography: Metrology and Properties*, vol. 3, 02 2015.

[9] S. Cattini, L. D. Cecilia, L. Ferrari, and L. Rovati, "Optical characterization of the beams generated by 3-d lidars: Proposed procedure and preliminary results on mrs1000," *IEEE Transactions on Instrumentation and Measurement*, vol. 69, no. 10, pp. 7796–7804, 2020.

[10] S. Cattini, L. Rovati, L. Di Cecilia, and L. Ferrari, "Comparison of the vlp-16 lidar system with an absolute interferometer," in *2020 IEEE International Instrumentation and Measurement Technology Conference (I2MTC)*, 2020, pp. 1–6.

[11] S. Cattini, D. Cassanelli, L. D. Cecilia, L. Ferrari, and L. Rovati, "A procedure for the characterization and comparison of 3-d lidar systems," *IEEE Transactions on Instrumentation and Measurement*, vol. 70, pp. 1–10, 2021.

[12] JCGM 106:2012, *Evaluation of measurement data — The role of measurement uncertainty in conformity assessment*. Pavillon de Breteuil F-92312 Sevres, Cedex, France: Joint Committee for Guides in Metrology, 2012. [Online]. Available: https://www.bipm.org/utils/common/documents/jcgm/JCGM_106_2012_E.pdf

[13] A. Mammeri, T. Zuo, and A. Boukerche, "Extending the detection range of vision-based vehicular instrumentation," *IEEE Transactions on Instrumentation and Measurement*, vol. 65, no. 4, pp. 856–873, 2016.

[14] S. Cattini and L. Rovati, "A simple calibration method to quantify the effects of head movements on vision-based eye-tracking systems," in *2016 IEEE International Instrumentation and Measurement Technology Conference Proceedings*, 2016, pp. 1–6.

[15] H. Lee and H. Huang, "A low-cost and noninvasive system for the measurement and detection of faulty streetlights," *IEEE Transactions on Instrumentation and Measurement*, vol. 64, no. 4, pp. 1019–1031, 2015.

[16] J. Li, H. He, H. He, L. Li, and Y. Xiang, "An end-to-end framework with multi-source monitoring data for bridge health anomaly identification," *IEEE Transactions on Instrumentation and Measurement*, vol. 70, pp. 1–9, 2021.

[17] S. Cattini and L. Rovati, "Low-cost imaging photometer and calibration method for road tunnel lighting," *IEEE Transactions on Instrumentation and Measurement*, vol. 61, no. 5, pp. 1181–1192, May 2012.